Residual dipolar couplings between quadrupolar nuclei in high resolution solid state NMR: Description and observations in the high-field limit

Sungsool Wi and Lucio Frydman[a)]
Department of Chemistry, University of Illinois at Chicago, 845 West Taylor Street, Chicago, Illinois 60607

(Received 9 September 1999; accepted 22 October 1999)

Nonsecular dipolar couplings between spin-$\frac{1}{2}$ nuclei that are in close proximity to quadrupolar spins have been extensively documented in solid state nuclear magnetic resonance (NMR), particularly when involving directly bonded $S={}^{13}\mathrm{C}$, $I={}^{14}\mathrm{N}$ spin pairs. These couplings arise due to the quadrupole-induced tilting of I's nuclear spin quantization axes, and their most notable characteristic is that they cannot be entirely averaged away by conventional magic-angle-spinning (MAS). Nonsecular dipolar couplings can also be expected to arise when both I and S are quadrupolar nuclei, even if these have hitherto not been analyzed in detail due to the interfering effects brought about by first- and second-order quadrupolar anisotropies. Yet, the advent of new high resolution techniques for studying half-integer quadrupole nuclei in solids such as multiple-quantum MAS or dynamic-angle-spinning can change this state of affairs. The present study presents a theoretical and numerical analysis on the results that can be expected from these techniques when applied to the observation of homonuclear or heteronuclear quadrupolar spin pairs in the high field limit. Variable field multiple-quantum MAS NMR results are then presented for a variety of compounds possessing ${}^{11}\mathrm{B}-{}^{14}\mathrm{N}$, ${}^{11}\mathrm{B}-{}^{11}\mathrm{B}$ and ${}^{55}\mathrm{Mn}-{}^{55}\mathrm{Mn}$ spin pairs, that validate these theoretical predictions and illustrate the valuable information that can be extracted from analyzing these residual MAS couplings. The research potential as well as resolution limitations that according to theoretical calculations these effects will impart on MQMAS spectra recorded at low or moderate magnetic fields are thus evidenced.
[S0021-9606(00)02503-4]

I. INTRODUCTION

The advent of magic-angle-spinning (MAS) has enabled the widespread application of NMR to the analysis of spin-$\frac{1}{2}$ nuclei in solids.[1] By averaging away all magnetic spin anisotropies that transform as second-rank tensors, sufficiently rapid MAS can in principle afford high resolution powder NMR spectra from these nuclei akin to those arising from molecules dissolved in an isotropic solution.[2,3] An important exception to this total averaging rule arises when the spin-$\frac{1}{2}$ nucleus under observation (S) is dipole-coupled to a neighboring quadrupole nucleus $I \geqslant 1$.[4,5] MAS averaging will then fail by itself to completely remove the dipolar anisotropies, due to the appearance of higher-order quadrupolar/dipolar cross correlation effects which no longer transform as second-order Legèndre polynomials. Such nonsecular effects were initially reported by vanderHart *et al.* on the ${}^{1}\mathrm{H}$ NMR spectra of static samples,[6] and subsequently became the focus of extensive attention due to the residual splittings that they originate in the ${}^{13}\mathrm{C}$ MAS NMR spectra of ${}^{14}\mathrm{N}$-containing polymers and biomolecules.[7,8] From a theoretical standpoint most of the initial efforts to analyze these phenomena centered on a combination of the physical principles laid by the static proton analysis and of numerical calculations that accounted for the MAS time evolution;[9,10] subsequent work by Olivieri and co-workers yielded an analytical description of this effect which further clarified the relations between the observed splittings and the parameters that determine them.[11–13] These included the spin number I, the internuclear distance r_{IS}, the isotropic and anisotropic indirect coupling constants J and ΔJ, the Larmor frequency of the I spin ω_I^0, its quadrupole parameters e^2qQ/h and η_Q, and the Euler angles (α, β) defining the orientation of the S-I internuclear vector in the principal axis system (PAS) of I's quadrupolar tensor.

In principle, nonsecular dipole effects should also be present in the NMR spectra of $S \geqslant 1$ nuclei; i.e., when both spins in the pair are quadrupolar. By contrast with the $S=\frac{1}{2}$, $I \geqslant 1$ case one could conceive dealing in this situation with I,S species that are of either a hetero- or a homonuclear nature. The analysis of such nonsecular couplings between quadrupoles has so far been a topic of only occasional interest,[14] probably reflecting the fact that MAS NMR spectra of $S \geqslant 1$ nuclei are usually dominated by quadrupole effects that easily mask the smaller residual dipolar interactions. Nevertheless, the advent of new high resolution techniques capable of affording isotropic NMR spectra for half-integer quadrupolar nuclei in powdered samples (Fig. 1)[15–17] opens up new opportunities for both the observation and exploitation of the valuable information carried by these

a)Author to whom correspondence should be addressed; Department of Chemistry (M/C 111), University of Illinois at Chicago, 845 W. Taylor Street, Room 4500, Chicago, IL 60607-7061; telephone: (312) 413-1053, FAX: (312) 996-0431; e-mail: lucio@samson.chem.uic.edu

nonsecular dipolar couplings. The present paper explores these potentials by introducing a theoretical description of these couplings in both homo- and heteronuclear spin pair systems. The predictions that arise from these theoretical derivations are then employed to derive the spectral results that can be expected from multiple-quantum (MQ) MAS, dynamic-angle-spinning (DAS) and double-rotation (DOR) NMR experiments using both numerical simulations as well as analytical procedures. The easily observable consequences of these effects are experimentally demonstrated at a variety of magnetic fields strengths, via analyses of the uni-and bi-dimensional MQMAS line shapes that they originate in a series of model organoboron and bismanganese complexes. It is worth adding that although attention in this work will be focused on the line shapes that arise from such compounds containing well-isolated homo- and heteronuclear spin pairs, Wimperis and co-workers have very recently noted that such effects can also be detected as field-dependent line broadenings in the MQMAS spectra of heteronuclear spin clusters possessing large quadrupole couplings (e.g., $NaBrO_3$).[18]

II. EXPERIMENT

Before discussing the effects that residual dipolar couplings can have on the high resolution solid state NMR spectra of quadrupole nuclei we briefly summarize the experimental procedures that were adopted for their subsequent verification. The compounds chosen for analysis are depicted in Scheme 1 showing in bold letters the relevant spin pairs whose couplings were explored;

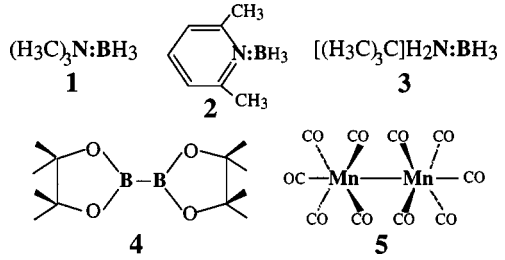

they include three amine-borane complexes incorporating directly bonded $^{11}B(S)-^{14}N(I)$ spin pairs that were used for monitoring residual heteronuclear effects, plus diborane and bismanganese complexes that were employed to monitor the homonuclear nuclear coupling effects in spin-$\frac{3}{2}$ ($I=S=^{11}B$) and spin-$\frac{5}{2}$ ($I=S=^{55}Mn$) systems, respectively. Because of their relative instability, all borane complexes were suitably purified by sublimation directly prior to their spectroscopic use. Our experimental analyses focused on the acquisition of 1D MAS and 2D MQMAS NMR spectra,[19] these were collected on laboratory-built 4.7 and 7.1 T NMR spectrometers using 4 and 5 mm doubly tuned probeheads and spinning rates $\omega_r/2\pi$ in the 6–10 kHz range. The ^{11}B and ^{55}Mn radio frequency fields afforded by these systems were in the order of 90–100 kHz, and all ^{11}B NMR spectra were acquired in the presence of ~80 kHz proton decoupling fields for the sake of improving the line's resolution. In order to maximize the MQMAS signal-to-noise optimized triple-quantum excitation and $3Q\rightarrow 1Q$ fast-amplitude-modulation conversion pulses were used;[19,20] the former usually resulted 4–6 μs long while the latter were chosen of the form $[(\delta)_x(\delta)_{\bar{x}}]_m$, with $\delta=0.8-1.2$ μs and m ranging from 2 to 5 as set on an empirical basis for each sample. Additional precautions that were taken for characterizing these new and relatively small spin coupling effects included the removal of mixed-phase distortions via the separate acquisition and suitable recombination of echo and antiecho MQMAS signals,[21] and the collection of sufficiently large 2D data sets to ensure a complete natural decay of the signals (usually 10–20 ms along both time domains). As follows from the detailed comparisons below, all these procedures enabled us to analyze the final experimental results without the need to consider potential nonidealities arising from the pulse sequence and with a frequency resolution that according to simulations we estimate at or below 15 Hz.

III. GENERAL THEORY

Although our emphasis will end up focusing on the results that can be observed on using the MQMAS technique for analyzing dipole-coupled pairs of quadrupolar spins in powdered samples, it is preferable to derive first the general form of the interaction Hamiltonian whose detection we will attempt during such experiments. Toward this end we begin by considering two nuclei I and S, both of them quadrupolar, that are mutually coupled. In the usual laboratory frame their total Hamiltonian is thus given by[22]

$$H_{\mathrm{Lab}}=H_I^Z+H_S^Z+H_I^Q+H_S^Q+H_{IS}^D+H_{IS}^J+H_I^{CS}+H_S^{CS}, \qquad (1)$$

where the first two terms on the right-hand side are the (dominant) Zeeman couplings of both spins, the second pair of terms are their local quadrupolar interactions, the following pair of terms account for their direct and indirect spin–spin couplings, and the last two terms denote their chemical shifts. Because of the complexity of Eq. (1) it is convenient to introduce two simplifications that will not seriously detract from the generality of the remaining treatment; namely, we will assume that the direct (D) and indirect (J) spin coupling tensors are coincident, and we will disregard for the time being the effects of the chemical shifts. The first of these assumptions is done on a heuristical basis as there is little or no evidence to bear on its contrary;[23] the second one is done as a matter of convenience at this stage, even if isotropic chemical shifts will show up and be accounted for later in the analysis. The explicit form of the remaining interactions in Eq. (1) can be best summarized in terms of irreducible tensor representations, which in their respective principal axes systems (PASs) are[24]

$$H_X^Z=\omega_X^O X_z, \quad X=I,S, \qquad (2)$$

$$H_X^Q=\sum_{m=-2}^{2}(-1)^m T_{2,-m}^{Q,X}\rho_{2,m}^{Q,X}, \quad X=I,S, \qquad (3)$$

$$H_{IS}=H_{IS}^D+H_{IS}^J=J\bar{I}\cdot\bar{S}+\sum_{m=-2}^{2}(-1)^m T_{2,-m}^{D}\rho_{2,m}^{D_{\mathrm{eff}}}. \qquad (4)$$

Here ω_X^0 ($X=I,S$) are the individual Larmor frequencies of the two spins, and the spin parts of the quadrupolar Hamiltonians are defined as

$$T_{2,0}^{Q,X}=\frac{eQ_x}{2X(2X-1)\hbar}[3X_z^2-X(X+1)], \tag{5a}$$

$$T_{2,\pm 1}^{Q,X}=\mp\frac{\sqrt{6}eQ_x}{4X(2X-1)\hbar}(X_zX_\pm+X_\pm X_z), \tag{5b}$$

$$T_{2,\pm 2}^{Q,X}=\pm\frac{\sqrt{6}eQ_x}{4X(2X-1)\hbar}X_\pm^2, \tag{5c}$$

with X representing either I or S, and the corresponding spatial elements are

$$\rho_{2,0}^{Q,X}=\tfrac{1}{2}eq_x, \tag{6a}$$

$$\rho_{2,\pm 1}^{Q,X}=0, \tag{6b}$$

$$\rho_{2,\pm 2}^{Q,X}=\frac{eq_x}{2\sqrt{6}}\eta_{Q,x}. \tag{6c}$$

The total coupling Hamiltonian H_{IS} [Eq. (4)] depends on an isotropic J term and on products of two-spin tensor elements

$$T_{2,0}^{D}=\frac{(3I_zS_z-\overline{I}\cdot\overline{S})}{\sqrt{6}}, \tag{7a}$$

$$T_{2,\pm 1}^{D}=\frac{I_zS_\pm+I_\pm S_z}{\mp 2}, \tag{7b}$$

$$T_{2,\pm 2}^{D}=\frac{I_\pm S_\pm}{2}, \tag{7c}$$

with the spatial elements

$$\rho_{2,0}^{D_{\rm eff}}=\sqrt{\frac{3}{2}}\left[\frac{-2\hbar\gamma_I\gamma_S}{r_{IS}^3}+\frac{2}{3}(J_\parallel-J_\perp)\right], \tag{8a}$$

$$\rho_{2,\pm 1}^{D_{\rm eff}}=0, \tag{8b}$$

$$\rho_{2,\pm 2}^{D_{\rm eff}}=0. \tag{8c}$$

The various interaction coupling parameters in these expressions (eQ, eq, η_Q, etc.) have their usual meaning,[24,25] and the explicit relations between the principal elements $\{\rho_{e,m}^{\lambda}\}$ and their spatial counterparts in a general frame $\{R_{e,m}^{\lambda}\}$ will be unambiguously established later on.

To calculate the NMR spectra resulting from these interactions on either heteronuclear (S detected) or homonuclear ($S+I$ observed) NMR experiments, it is customary to remove the dominant Zeeman effects by going into an interaction representation. The resulting frame rotates at the Larmor frequencies of the two spins as driven by the propagator

$$U(t)=\exp[-i(\omega_S^0S_z+\omega_I^0I_z)t], \tag{9}$$

which imparts into $H_{\rm Lab}$ the time dependence

$$\tilde{H}_{\rm Lab}(t)=U\cdot H_{\rm Lab}\cdot U^{-1}+\frac{dU}{dt}\cdot U^{-1}. \tag{10}$$

Average Hamiltonian theory can then be applied to obtain a time-independent rendering of this rotating-frame interaction according to

$$\overline{H}=H^{(1)}+H^{(2)}+\ldots, \tag{11}$$

where

$$H^{(1)}=\frac{1}{\tau_c}\int_0^{\tau_c}\tilde{H}_{\rm Lab}(t)dt \tag{12}$$

$$H^{(2)}=\frac{-i}{2\tau_c}\int_0^{\tau_c}dt\int_0^t[\tilde{H}_{\rm Lab}(t),\tilde{H}_{\rm Lab}(t')]dt', \tag{13}$$

and $\tau_c=\max[(2\pi/\omega_I^O),(2\pi/\omega_S^0)]$ is a sufficiently long cycle time for the secular Zeeman truncations to take place. The Hamiltonians that need to be dealt with in these time-dependent expressions are of the type

$$\tilde{H}_X^Q(t)=\frac{\sqrt{6}eQ_X}{4X(2X-1)\hbar}\left\{\begin{array}{c}R_{2,-2}^{Q,X}X_+^2e^{2i\omega_X^Qt}+R_{2,-1}^{Q,X}X_+(2X_z+1)e^{i\omega_X^Qt}+\frac{2}{\sqrt{6}}R_{2,0}^{Q,X}\{3X_z^2-X(X+1)\}\\ -R_{2,1}^{Q,X}X_-(2X_z-1)e^{-i\omega_X^Qt}+R_{2,2}^{Q,X}X_-^2e^{-2i\omega_X^Qt}\end{array}\right\}\quad X=I,S \tag{14}$$

and

$$\begin{aligned}\overline{H}_{IS}(t)=&\left(J+\sqrt{\frac{2}{3}}R_{2,0}^{D_{\rm eff}}\right)I_zS_z+\left(\frac{1}{2}J-\frac{1}{2\sqrt{6}}R_{2,0}^{D_{\rm eff}}\right)\\&\times(I_+S_-e^{i\omega_I^0t}e^{-i\omega_S^0t}+I_-S_+e^{-i\omega_I^0t}e^{i\omega_s^0t})\\&+\frac{1}{2}R_{2,-1}^{D_{\rm eff}}(I_zS_+e^{i\omega_S^0t}+I_+S_ze^{i\omega_I^0t})\\&-\frac{1}{2}R_{2,1}^{D_{\rm eff}}(I_zS_-e^{-i\omega_S^0t}+I_-S_ze^{-i\omega_I^0t})\\&+\frac{1}{2}R_{2,-2}^{D_{\rm eff}}I_+S_+e^{i\omega_I^0t}e^{i\omega_S^0t}\\&+\frac{1}{2}R_{2,2}^{D_{\rm eff}}I_-S_-e^{-i\omega_I^0t}e^{-i\omega_S^0t}.\end{aligned} \tag{15}$$

Evidently, $H^{(1)}$ in Eq. (11) will involve simple time averages of the various coupling interactions appearing in Eq. (1). If one is dealing with a heteronuclear pair and is interested solely on the S spin observation these secular first-order terms will be

$$\begin{aligned}H_{\rm hetero}^{(1)}=&\frac{eQ_s}{2S(2S-1)\hbar}R_{2,0}^{Q,S}[3S_z^2-S(S+1)]\\&+\left(J+\sqrt{\frac{2}{3}}R_{2,0}^{D_{\rm eff}}\right)I_zS_z,\end{aligned} \tag{16}$$

whereas for a homonuclear case with simultaneous I,S observation these will involve

$$H^{(1)}_{\text{homo}}=\frac{eQ_s}{2S(2S-1)\hbar}R^{Q,S}_{2,0}[3S_z^2-S(S+1)]+\frac{eQ_I}{2I(2I-1)\hbar}R^{Q,I}_{2,0}[3I_z^2-I(I+1)]+\left(J+\sqrt{\frac{2}{3}}R^{D_{\text{eff}}}_{2,0}\right)I_zS_z+\left(\frac{1}{2}J-\frac{1}{2\sqrt{6}}R^{D_{\text{eff}}}_{2,0}\right)\times(I_+S_-+I_-S_+). \quad (17)$$

In a complete high field limit, where Zeeman interactions truncate every other coupling, it is generally sufficient to consider these $H^{(1)}$ terms to account for the observable NMR spectra. When the quadrupole couplings of either I or S spins become sufficiently large, however, an appropriate description will demand the inclusion of all cross terms in Eq. (13) that involve the corresponding quadrupole Hamiltonian. In the terminology of static Rayleigh–Schroedinger perturbation theory, this is tantamount to accounting for the first-order corrections to the Zeeman eigenstates caused by the quadrupole-induced tilting of the spins' quantization axes.[26] The manner in which the various secular cross terms in the commutator $H^{(2)}$ will be evaluated, depends again on whether one is dealing with hetero- or homonuclear cases. Using Eqs. (14) and (15) it is possible to show that the former will lead to

$$H^{(2)}_{\text{hetero}}=H_S^{Q,Q}+H_{IS}^{Q_S,D}+H_{IS}^{Q_I,D}=3\left(\frac{eQ_S}{2S(2S-1)\hbar}\right)^2\frac{1}{\omega_S^0}\left\{\begin{array}{c}R^{Q,S}_{2,-1}R^{Q,S}_{2,1}S_z[4S(S+1)-8S_z^2-1]\\+R^{Q,S}_{2,-2}R^{Q,S}_{2,2}S_z[2S(S+1)-2S_z^2-1]\end{array}\right\}-\sqrt{\frac{3}{2}}\frac{eQ_I}{2I(2I-1)\hbar}\frac{1}{\omega_I^0}(R^{Q,I}_{2,-1}R^{D_{\text{eff}}}_{2,1}+R^{Q,I}_{2,1}R^{D_{\text{eff}}}_{2,-1})\{3I_z^2-I(I+1)\}S_z-\sqrt{\frac{3}{2}}\frac{eQ_S}{2S(2S-1)\hbar}\frac{1}{\omega_S^0}(R^{Q,S}_{2,-1}R^{D_{\text{eff}}}_{2,1}+R^{Q,S}_{2,1}R^{D_{\text{eff}}}_{2,-1})\{3S_z^2-S(S+1)\}I_z \quad (18)$$

in heteronuclear systems, and to

$$H^{(2)}_{\text{homo}}=H_S^{Q,Q}+H_I^{Q,Q}+H_{IS}^{Q_S,D}+H_{IS}^{Q_I,D}=3\left(\frac{eQ_S}{2S(2S-1)\hbar}\right)^2\frac{1}{\omega_S^0}\left\{\begin{array}{c}R^{Q,S}_{2,-1}R^{Q,S}_{2,1}S_z[4S(S+1)-8S_z^2-1]\\+R^{Q,S}_{2,-2}R^{Q,S}_{2,2}S_z[2S(S+1)-2S_z^2-1]\end{array}\right\}+3\left(\frac{eQ_I}{2I(2I-1)\hbar}\right)^2\frac{1}{\omega_I^0}\left\{\begin{array}{c}R^{Q,I}_{2,-1}R^{Q,I}_{2,1}I_z[4I(I+1)-8I_z^2-1]\\+R^{Q,I}_{2,-2}R^{Q,I}_{2,2}I_z[2I(I+1)-2I_z^2-1]\end{array}\right\}-\sqrt{\frac{3}{2}}\frac{eQ_S}{2S(2S-1)\hbar}\frac{1}{\omega_S^0}(R^{Q,S}_{2,-1}R^{D_{\text{eff}}}_{2,1}+R^{Q,S}_{2,1}R^{D_{\text{eff}}}_{2,-1})\times\{3S_z^2-S(S+1)\}I_z-\sqrt{\frac{3}{2}}\frac{eQ_I}{2I(2I-1)\hbar}\frac{1}{\omega_I^0}(R^{Q,I}_{2,-1}R^{D_{\text{eff}}}_{2,1}+R^{Q,I}_{2,1}R^{D_{\text{eff}}}_{2,-1})S_z\{3I_z^2-I(I+1)\}+\frac{1}{2}\sqrt{\frac{3}{2}}\frac{eQ_S}{2S(2S-1)\hbar}\frac{1}{\omega_S^0}(R^{Q,S}_{2,-1}R^{D_{\text{eff}}}_{2,1}+R^{Q,S}_{2,-2}R^{D_{\text{eff}}}_{2,2})S_+I_-(2S_z+1)+\frac{1}{2}\sqrt{\frac{3}{2}}\frac{eQ_S}{2S(2S-1)\hbar}\frac{1}{\omega_S^0}(R^{Q,S}_{2,1}R^{D_{\text{eff}}}_{2,-1}+R^{Q,S}_{2,2}R^{D_{\text{eff}}}_{2,-2})S_-I_+(2S_z-1)+\frac{1}{2}\sqrt{\frac{3}{2}}\frac{eQ_I}{2I(2I-1)\hbar}\frac{1}{\omega_I^0}(R^{Q,I}_{2,-1}R^{D_{\text{eff}}}_{2,1}+R^{Q,I}_{2,-2}R^{D_{\text{eff}}}_{2,2})S_-I_+(2I_z+1)+\frac{1}{2}\sqrt{\frac{3}{2}}\frac{eQ_I}{2I(2I-1)\hbar}\frac{1}{\omega_I^0}(R^{Q,I}_{2,1}R^{D_{\text{eff}}}_{2,-1}+R^{Q,I}_{2,2}R^{D_{\text{eff}}}_{2,-2})S_+I_-(2I_z-1) \quad (19)$$

in homonuclear ones. These equations allow one to deduce the effects that residual quadrupole/quadrupole and quadrupole/dipole cross correlations will have in a variety of NMR experiments, provided that quadrupole coupling constants remain small enough for the two-term expansion in Eq. (11) to stay valid. Should this cease to be the case a full numerical diagonalization approach would have to be adopted,[27] such procedure is outside the scope of this mainly high-field-limit work. Also worth noting is the substantial differences that even under this high field assumption characterize the hetero- and homonuclear scenarios, both in the complexity of their Hamiltonians and in the approach that these will demand for further calculating their NMR spectra. Because of these differences we break up the rest of this discussion into a heteronuclear treatment, pursued to a further extent due to its simpler and more ammenable nature, and a homonuclear treatment that is mainly restricted to MQMAS calculations and experiments on pairs of spin-$\frac{3}{2}$ and spin-$\frac{5}{2}$ nuclei.

IV. RESIDUAL HETERONUCLEAR COUPLINGS IN MQMAS, DAS AND DOR NMR

A. Theoretical analysis of high-field MQMAS spectra

The potential effects that J couplings between S and I spins may have on the MQMAS NMR line shapes of the S nucleus have been recently discussed for the case $I=\frac{1}{2}$.[28] We

extend in this paragraph such discussion to a case where I is quadrupolar, and can thus also be interacting via the residual dipolar coupling effects introduced above. Before doing so, however, we briefly dwell on the nature of MQMAS acquisitions so as to lay the foundations of the subsequent discussions and derivations. As explained elsewhere in detail,[19,29] MQMAS is a 2D NMR experiment capable of providing high resolution NMR spectra from half-integer quadrupole nuclei even when these are in powder samples. This is done by correlating pairs of $+m \leftrightarrow -m$(MQ) and $+\frac{1}{2} \leftrightarrow -\frac{1}{2}$ ($1Q$) transition frequencies within the S spin manifold, while subjecting the sample to a fast mechanical spinning at an angle $\theta_s = 54.7°$ with respect to the magnetic field B_0 [Fig. 1(A)]. Both domains in such an experiment are affected by second-order quadrupolar anisotropies, yet the anisotropic shifts that result for the MQ and $1Q$ transitions are proportional to one another for each and every crystallite in the powder. The ratio between these anisotropies is given by a rational number $k = |C_S^4(m)|/C_S^4(1/2)$, where

$$C_S^4(m_S) = 2m_S[18S(S+1) - 34m_S^2 - 5]. \tag{20}$$

is a polynomial depending on the eigenstates m_S being correlated and on the number S of the spin being analyzed. The fact that this ratio is independent of site or crystallite properties can be exploited to cancel out the quadrupole anisotropies along one of the two spectral domains, and thus obtain a unidimensional high resolution NMR projection regardless of sample characteristics. This canceling of anisotropies requires subjecting the 2D MQMAS NMR results to some form of shearing transformation. Different strategies have been discussed and illustrated for carrying out such transformation;[19,30] here we will assume that it merely involves a mathematical procedure such as

$$I(\nu_1, \nu_2) \rightarrow I(\nu_1 + \nu_2 |C_S^4(m)|/C_S^4(\tfrac{1}{2}), \nu_2) \tag{21}$$

following the acquisition of the data.

In view of these basic considerations it follows that a possible way for calculating the effects of residual heteronuclear interactions on MQMAS experiments is by computing the Fourier transform of the time-domain signal

$$S(t_1, t_2) = \sum_{\substack{\text{All} \\ \text{eigenstates}}} \sum_{m_I} \left\{ \int_{\text{powder}} \exp[i\langle E(m, m_I) - E(-m, m_I)\rangle t_1] \times \exp[i\langle E(\tfrac{1}{2}, m_I) - E(-\tfrac{1}{2}, m_I)\rangle t_2] d\Omega \right\}, \tag{22}$$

where the $\langle ... \rangle$ brackets indicate the averaging effects introduced by the MAS. This equation exploits the fact that since $H^{(1)}$ and $H^{(2)}$ are only functions of the I_z and S_z operators their eigenvalues can be found in the conventional Zeeman product basis set

$$(H^{(1)} + H^{(2)}_{\text{hetero}})|m_S, m_I\rangle = E(m_S, m_I)|m_S, m_I\rangle;$$
$$-S \leqslant m_S \leqslant S; -I \leqslant m_I \leqslant I. \tag{23}$$

Notice also that out of the various contributions to $H^{(1)}$ all but the isotropic J and chemical shift couplings can be disregarded on considering the final eigenvalues, as first-order dipolar, quadrupolar and shielding anisotropies do not play relevant parts in the MQMAS experiments to be analyzed.

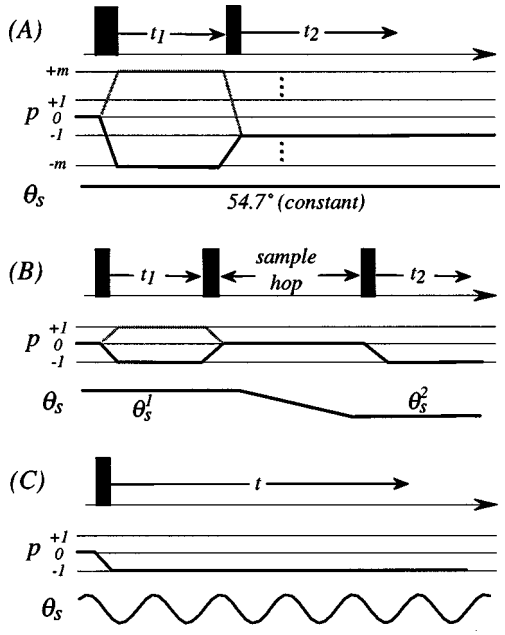

FIG. 1. Different experimental approaches available to the acquisition of high resolution solid NMR spectra from half-integer quadrupolar nuclei: (A) MQMAS; (B) DAS; (C) DOR.

Computing the effects of sample spinning on such eigenvalues, not just for the fast MAS case but for arbitrary spinning speeds and angles, demands that the spatial parts of all relevant interactions be expressed into a common reference frame. Common transformations thus need to be defined for all the couplings introduced in Eqs. (2)–(4). In the present study we defined the various sets of Euler angles that are involved in these principal axes transformations according to

$$EFG(I) \underset{(a,b,c)}{\rightarrow} D \underset{(\alpha,\beta,\gamma)}{\rightarrow} EFG(S) \underset{(\varphi,\theta,\xi)}{\rightarrow} ROTOR \underset{(\omega_r t, \theta_s, 0°)}{\rightarrow} LAB, \tag{24}$$

where $EFG(I,S)$ denotes the PASs of the electric field gradient tensors for each of the quadrupolar nuclei, D denotes the coinciding uniaxial dipolar- and J-coupling tensors, *ROTOR* refers to a frame of reference mounted on the spinning sample, and *LAB* is a system whose z-axis coincides with the direction of the magnetic field B_0. With these definitions the spatial coefficients of the various Hamiltonian terms can be written in terms of their principal value components [Eqs. (6) and (8)] as

$$R_{2,m}^{Q,S} = \sum_{k=-2}^{2} \sum_{n=-2}^{2} D_{k,m}^2(\omega_r t, \theta_s, 0°) D_{n,k}^2(\varphi, \theta, \xi) \rho_{2,n}^{Q,S}, \tag{25}$$

$$R_{2,m}^{D_{\text{eff}}} = \sum_{k=-2}^{2} \sum_{n=-2}^{2} \sum_{p=-2}^{2} D_{k,m}^2(\omega_r t, \theta_s, 0°) D_{n,k}^2(\varphi, \theta, \xi) \times D_{p,n}^2(\alpha, \beta, \gamma) \rho_{2,p}^{D_{\text{eff}}}, \tag{26}$$

$$R_{2,m}^{Q,I}=\sum_{k=-2}^{2}\sum_{n=-2}^{2}\sum_{p=-2}^{2}\sum_{q=-2}^{2}D_{k,m}^{2}(\omega_r t,\theta_s,0^\circ)\times D_{n,k}^{2}(\varphi,\theta,\xi)D_{p,n}^{2}(\alpha,\beta,\gamma)D_{q,p}^{2}(a,b,c)\rho_{2,q}^{Q,I}, \tag{27}$$

where in all cases $m=\pm1,\pm2$. In these expressions $D_{m,n}^{2}(x,y,z)$ denote Wigner rotation matrices fulfilling

$$D_{m,n}^{2}(x,y,z)=d_{m,n}^{2}(y)e^{-i(mx+nz)} \tag{28}$$

with the reduced matrix $d_{m,n}^{2}(y)$ as defined by Wigner's formula. Except for the special case $\theta_s=0^\circ$, sample spinning will make all the spin interactions in Eqs. (25)–(27) oscillatory time dependent. Thus to pursue this analysis these time dependencies need to be explicitly evaluated for each of the relevant interactions as well as for their mutual cross terms; an outline of these lengthy but straightforward calculations is presented in the Appendix.

Rather than programming the resulting equations numerically and obtaining a computational prediction of the residual dipolar effects for arbitrary spinning and coupling conditions, we decided to pursue first an analytical path focused on the centerbands that can be expected from fast-spinning or rotor-synchronized MQMAS experiments. This requires calculating for all the spatial terms in the Hamiltonian the rotor period average

$$\langle H_{\text{hetero}}^{(2)}\rangle=\frac{\omega_r}{2\pi}\int_0^{2\pi/\omega_r}H_{\text{hetero}}^{(2)}(t)dt. \tag{29}$$

Under these conditions the eigenvalues E defining the S-spin energy levels can be written as

$$\begin{aligned}\langle E(m_S,m_I)\rangle=&\frac{3}{\omega_0^s}\left[\frac{eQ_s}{2S(2S-1)\hbar}\right]^2\\&\times\left\{\begin{array}{l}\langle R_{2,-1}^{Q,S}R_{2,1}^{Q,S}\rangle m_S[4S(S+1)-8m_s^2-1]+\\ \langle R_{2,-2}^{Q,S}R_{2,2}^{Q,S}\rangle m_s[2S(S+1)-2m_s^2-1]\end{array}\right\}\\&+Jm_sm_I-\sqrt{\frac{3}{2}}\left[\frac{eQ_I}{2I(2I-1)\hbar\omega_0^I}\right]\\&\times\langle R_{2,-1}^{Q,I},R_{2,1}^{D_{\text{eff}}}+R_{2,1}^{Q,I}R_{2,-1}^{D_{\text{eff}}}\rangle\\&\times m_S[3m_I^2-I(I+1)],\end{aligned} \tag{30}$$

where the time averages of the various $\langle R_{2,m}^{\lambda}R_{2,-m}^{\lambda}\rangle$ angular dependencies are summarized in Eqs. (A11)–(A13) of the Appendix, and we have exploited the fact that all terms in the Hamiltonian commute with one another to disregard potential higher order effects. The first term in this eigenvalue expression represents S's second-order quadrupolar frequencies. Its resulting line shapes under a variety of variable-angle and magic-angle-spinning conditions have been extensively described;[31,32] in MQMAS, these effects are known to be absent along the isotropic dimension. By contrast, the remaining terms are new in this quadrupolar context and will not be averaged out by either the MQ or the MAS procedures. It is interesting to note the formal resemblance between these new terms and the frequency expressions that have been previously derived for the residual dipolar couplings between a quadrupole nucleus and $S=\frac{1}{2}$.[33]

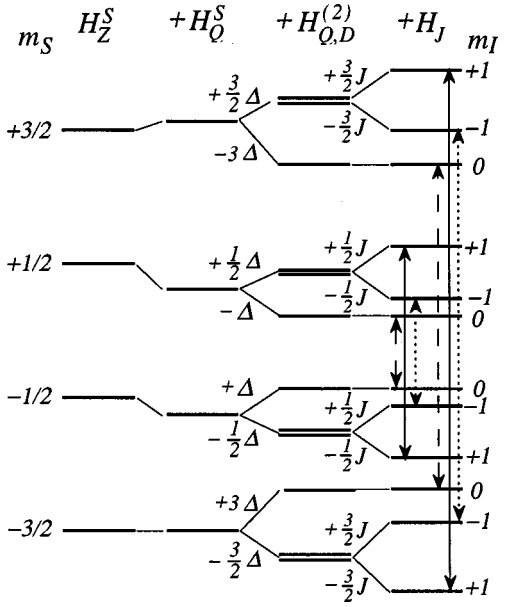

FIG. 2. Energy level diagram for an $S=\frac{3}{2}$ nucleus coupled to an $I=1$ spin, showing the hierarchical effects introduced by Zeeman, quadrupolar, residual dipolar and J-coupling interactions on the S-spin manifold. The various kinds of vertical arrows (—, - -, ·····) denote pairs of transitions connected by 2D MQMAS for different m_I spin states (+1, 0, −1, respectively); notice that the effects of the various spin interactions are not illustrated in a common energy scale.

Before employing these eigenvalue expressions to calculate the full 2D MQMAS line shapes it is illustrative to compute their overall powder averages, as these will lead to the isotropic splittings that will in turn characterize the residual dipolar effects along the isotropic MQMAS dimension.[4] This entails removing the anisotropic dependencies by calculating the weighted integral

$$\frac{\int_0^{2\pi}\int_0^{\pi}\langle R_{2,-1}^{Q,I}R_{2,1}^{D_{\text{eff}}}+R_{2,1}^{Q,I}R_{2,-1}^{D_{\text{eff}}}\rangle\sin\theta\,d\theta\,d\varphi}{\int_0^{2\pi}\int_0^{\pi}\sin\theta\,d\theta\,d\varphi}, \tag{31}$$

the remaining powder angle (ξ) being irrelevant as it denotes a rotor phase that was averaged away by the integration in Eq. (29), while the second-order quadrupole effects from Eq. (30) are naturally absent along this spectral axis. The result of implementing such powder averaging on the eigenvalue's expression is the zero-order energy shift

$$\langle E(m_S,m_I)\rangle=Jm_Im_S-\Delta[3m_I^2-I(I+1)]m_S, \tag{32}$$

where

$$\Delta=\frac{3}{20}\frac{D_{zz}^{\text{eff}}}{\omega_0^I}\left[\frac{e^2qQ_I}{2I(2I-1)h}\right](3\cos^2 b-1+\eta_Q^I\sin^2 b\cos 2a) \tag{33}$$

and

$$D_{zz}^{\text{eff}}=\sqrt{\frac{2}{3}}\rho_{2,0}^{D^{\text{eff}}}=-\frac{2\hbar\gamma_I\gamma_S}{r_{IS}^3}+\frac{2}{3}\Delta J. \tag{34}$$

This expression is analogous to the one derived by Olivieri *et al.* for the case $S=\frac{1}{2}$,[11,13] and it may be used to compute analytically the splittings to be expected from heteronuclear high-field MQMAS spectra involving arbitrary I,S spin pairs and MQ transition orders $m\leftrightarrow -m$. Thus for instance, a

schematic description of the modifications that will be introduced by these effects on the energy manifold of the simplest possible such case ($S=\frac{3}{2}, I=1$) is illustrated in Fig. 2. It shows that on top of the conventional Zeeman and quadrupole effects residual MAS dipolar couplings will split the energy levels of the S spin according to the $|m_I|$ values of the I spin, and then as a result of the J_{IS} further splittings can be expected between $+m_I$ and $-m_I$ states leading to an overall S multiplet composed by $2I+1$ different isotropic transitions. When considering that the observation of such isotropic splittings demands a shearing procedure like the one outlined in Eq. (21), it follows that in a general case multiplets arising in the high resolution MQMAS spectra of S will be positioned at frequencies

$$\nu_{\mathrm{iso}}(m_I)=\frac{[|C_S^4(m)|+2mC_S^4(\frac{1}{2})]}{C_S^4(\frac{1}{2})+|C_S^4(m)|}\times\{[3m_I^2-I(I+1)]\Delta+m_IJ\}, \tag{35}$$

where m denotes again the order of the S-spin MQ transition that has been used in the 2D NMR correlation. Clearly, measurements at varying magnetic fields (different ω_0^I) can enable one to separate the J from the dipolar (Δ) effects within this multiplet, and from there extract the information carried by these different couplings.

As a first test of these analytical expressions it is illustrative to compare their predictions with those that arise from a suitable numerical powder average of Eq. (30); i.e., from the MQMAS frequencies expected prior to a computation of the isotropic centers of mass. To obtain such numerical simulations complete 2D MQMAS data sets based on Eq. (22) were calculated, processed into purely absorptive 2D NMR line shapes, projected onto a sheared isotropic dimension, and then compared with the expectations of the analytical expressions. Illustrative results of these procedure are presented in Fig. 3 for a variety of cases; these clearly evidence that most of the information made available by MQMAS NMR projections is accurately summarized by the isotropic splittings derived from the analytical treatment.

In addition to these isotropic projections, MQMAS provides complete 2D line shapes from which further information related to this effect can be extracted. For each coupled chemical site in the sample these 2D line shapes will correlate the residual dipolar plus J couplings between S and I spins, dependent as shown in Eq. (33) on the Euler angles relating the PAS of I's EFG with the I-S internuclear vector, against the sum of these effects plus S's own second-order quadrupole frequency. The resulting 2D MQMAS line shapes can thus be expected sensitive to the relative orientation between the two quadrupolar tensors of the coupled spins. Numerical simulations validating such expectations are presented in Fig. 4 for I,S pairs possessing constant coupling parameters such as those assumed in Fig. 3 (left), but varying sets of relative tensor geometries.

B. Nonsecular heteronuclear couplings: Experimental MQMAS results

In order to test the theoretical predictions of the preceding paragraph a series of 2D MQMAS NMR experiments on

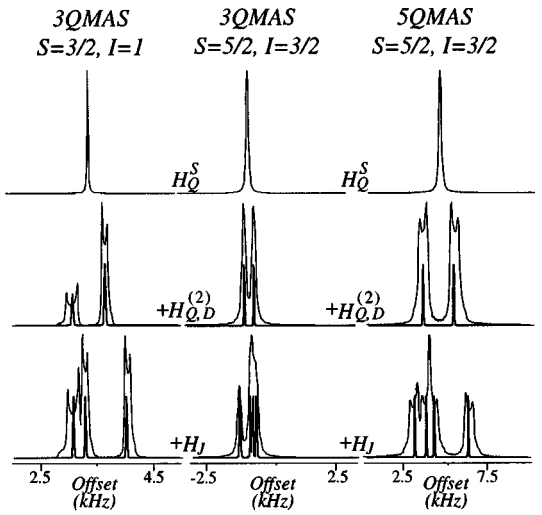

FIG. 3. Comparisons between the MQMAS line shapes predicted by the isotropic analytical expression given in Eq. (35), versus complete numerical calculations of 2D MQMAS spectra based on Eq. (22) and a subsequent shearing/projection onto an isotropic dimension. Peak shapes in the analytical traces are shown artificially thicker and scaled by a factor of 0.5; their multiplets intensities are proportional to the number of m_I components contributing to each transition and their linewidths were set to 10 Hz. In all cases tensors were assumed axially symmetric and coincident, the frequency scales refer to an isotropic shift $\delta_S=0$ kHz, and the cumulative effects of dipolar and J-couplings (fixed at 100 Hz) are shown in the second and third rows. Spectra on the left assumed 3QMAS NMR on an $S=\frac{3}{2}$ ($e^2qQ/h=2$ MHz, $\omega_0=64.4$ MHz) coupled to an $I=1$ ($e^2qQ/h=-3$ MHz, $\omega_0=14.5$ MHz) with a $D_{zz}^{\mathrm{eff}}=1.7$ kHz; the center and right columns describe the 3QMAS and 5QMAS spectra of an $S=\frac{5}{2}$ ($e^2qQ/h=3$ MHz, $\omega_0=52$ MHz) coupled to an $I=\frac{3}{2}$ ($e^2qQ/h=12$ MHz, $\omega_0=20$ MHz).

I,S quadrupolar spin pairs were carried out. Toward this end we found the directly bonded ^{14}N–^{11}B ($I=1, S=\frac{3}{2}$) pairs in aminoborane complexes suitable. In the presence of heteronuclear ^{1}H decoupling these compounds (Scheme 1) represent well-isolated I,S systems; in fact the relative sharpness of the ^{11}B MQMAS NMR features even in the absence of strong decoupling fields suggests active three-fold internal rotation of the $-BH_3$ groups that considerably attenuate their internal couplings at room temperature.[34] There are, however, certain disadvantages associated to this choice of compounds, including a relatively poor chemical stability and an unavailability of MQ orders higher then three for testing our predictions. To alleviate this last drawback measurements were repeated as a function of magnetic field strength, given the known dependencies that affect the relevant second-order $H^{Q,Q}$ and $H^{Q,D}$ cross-term effects. It may also be worth clarifying that this choice of compounds was dictated by suitability, availability and preliminary structural/magnetic resonance data, rather than for the sake of enhancing the ^{11}B NMR spectral resolution.

Figure 5 presents representative 4.7 and 7.1 T 2D experimental ^{11}B NMR spectra recorded on the trimethylamine borane complex (**1**, Scheme 1), and compares them with best fit simulations obtained on the basis of constant ^{11}B,^{14}N coupling parameters and of changing Larmor frequencies. Further comparisons between these experimental and theoretical results are illustrated in Fig. 6, which shows the 1D traces obtained upon projecting the 2D spectra onto their respective

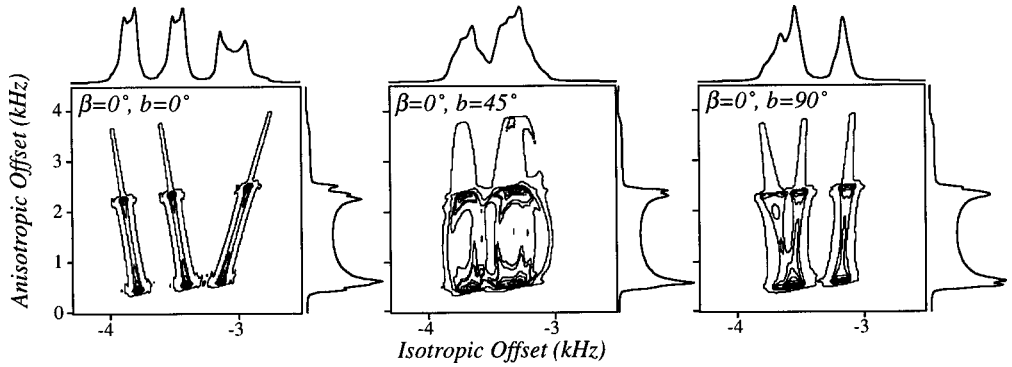

FIG. 4. Dipole-induced dependence of sheared 2D MQMAS *S*-spin line shapes on the relative orientations between *S* and *I* EFG coupling tensors. Spectra were calculated for a prototypical ^{11}B–^{14}N spin pair that is 1.5 Å apart and at 4.7 T assuming axially symmetric EFG's and $(e^2qQ/h)11_B=2$ MHz, $(e^2qQ/h)14_N=-3$ MHz, $J=100$ Hz, $\Delta J=0$ Hz. Vertical and horizontal spectra correspond to the anisotropic and isotropic projections of the 2D data sets, respectively.

isotropic and anisotropic MQMAS axes. In order to obtain these best fit simulations the B–N distance was assumed as in the compound's gas phase electron diffraction report (1.656 Å),[35] and the quadrupole asymmetry parameters were assumed null for both sites on the basis of molecular symmetry and of the ^{11}B MAS NMR line shapes. The former consideration constrained the system into collinear quadrupolar and dipolar PASs, i.e., $(\alpha,\beta)=(a,b)=(0°,0°)$. A simple analysis of the MQMAS center of mass along the two spectral dimensions[19] also yields the boron quadrupole coupling constant: $(e^2qQ/h)_{11_B}=(1.67\pm0.05)$ MHz. Subsequent refinement of the 2D powder features then yielded the quadrupolar and coupling parameters $(e^2qQ/h)_{14_N}=(-2.4\pm0.1)$ MHz, $J_{BN}=(20\pm10)$ Hz, $\Delta J\approx0$ Hz, and a natural line width for the ^{11}B powder pattern of 10 Hz. The quadrupole coupling constants thus obtained for both boron and nitrogen are systematically lower than those previously measured for this compound by microwave spectroscopy in the gas phase (2.06 and −2.83 MHz, respectively),[36] probably reflecting the tighter B–N bond occurring in the solid complex. Such differences notwithstanding the spectra of this compound clearly demonstrate the possibility of detecting these effects even at moderate magnetic fields, and of extracting from them meaningful information.

Figure 7 illustrates a similar ^{11}B MQMAS analysis, this time carried out at 4.7 T on a borane-lutidine sample (**2**, Scheme 1). As opposed to the previous case no literature parameters could be found for this compound, while the absence of three-fold symmetry around the B–N bond precluded many of the former's *a priori* simplifying assumptions. Boron quadrupole parameters can still become available from the center of mass of the 2D MQMAS line shape and from simulating its anisotropic projection. The overall residual dipolar effects are smaller here than in the trimethylamine complex; if one assumes that ^{14}N quadrupole coupling constants are equal in these two aducts, this feature

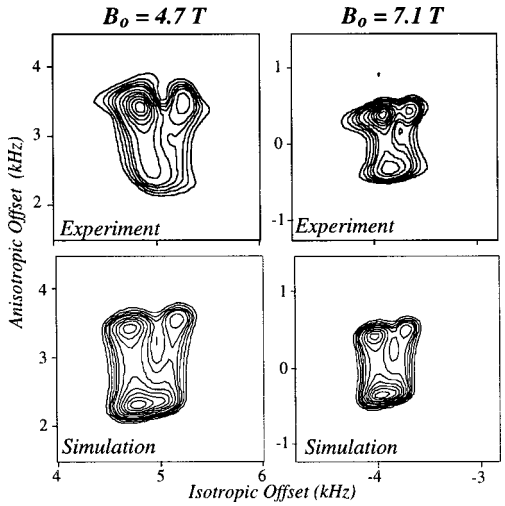

FIG. 5. Comparisons between the experimental 2D MQMAS line shapes observed for trimethylamine borane at magnetic fields of 4.7 and 7.1 T, and their best fits obtained as described in the text. ^{11}B Larmor frequencies at these fields were 64.49 and 96.77 MHz; the ^{14}N frequencies were 14.5 and 21.75 MHz, respectively.

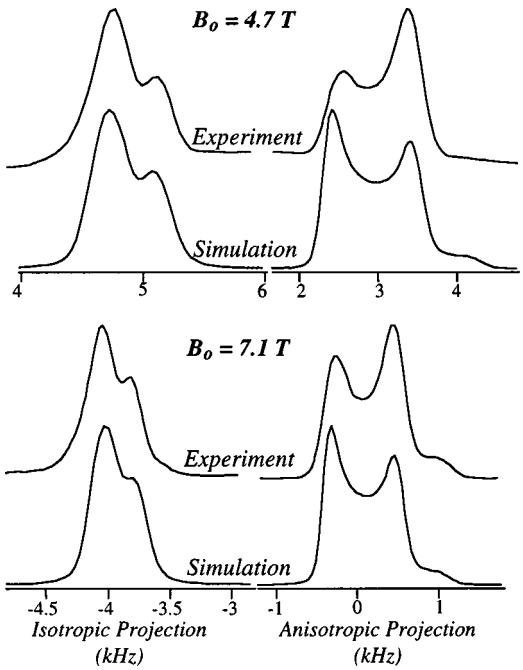

FIG. 6. Idem as in Fig. 5 but for the isotropic and anisotropic projections of the corresponding 2D MQMAS spectra.

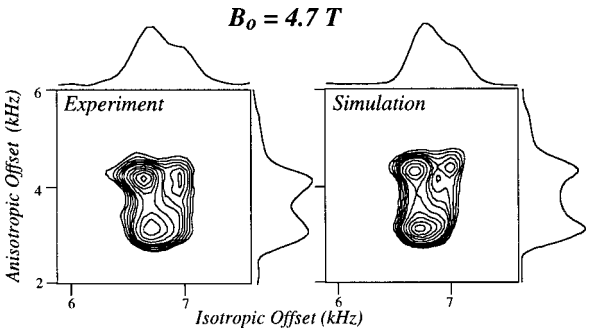

FIG. 7. Comparisons between experimental ^{11}B MQMAS results observed for a lutidine-borane complex at 4.7 T and simulations based on the following best fit parameters: $(e^2qQ/h)11_B = 1.8$ MHz, $(\eta_Q)11_B = 0.2$, $(e^2qQ/h)14_N = -2.0$ MHz, $r_{BN} = 1.78$ Å, $(\alpha,\beta) = (a,b) = (0°,0°)$, $J = 15$ Hz, $\Delta J = 0$, natural ^{11}B linewidths $= 10$ Hz. Vertical and horizontal traces correspond to the anisotropic and isotropic projections of the data.

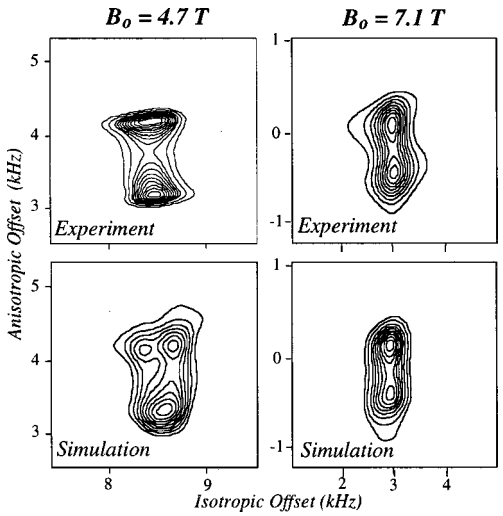

FIG. 8. Summary of the 4.7 and 7.1 T ^{11}B MQMAS NMR results obtained for a terbutilamine-borane complex, versus the simulated line shapes that can be expected on the basis of literature quadrupole coupling data and the trimethylamine B–N coupling parameters.

should then be ascribed to a lengthened B–N distance of 1.89 Å. In fact quantum chemical calculations have predicted a 0.05 Å increase in the B–N bond length on going from the trimethylamine- to the pyridine-borane complex;[37] the significantly longer distance that would be needed to simulate the lutidine-borane complex could then be rationalized as a result of further steric interactions between the methyl substituents of the pyridil group and the borane moiety. Alternatively, one could assume a constant (1.66 Å) B–N internuclear distance and deduce from the MQMAS spectra a -1.7 MHz ^{14}N quadrupole coupling constant. The actual ^{14}N and B–N coupling parameters that yielded a best fit were found in between these limiting cases; results of such numerical simulations are presented on the right-hand column of Fig. 7.

A final theoretical/experimental comparison on the results expected from MQMAS for these heteronuclear effects is presented in Fig. 8, which shows variable-field ^{11}B NMR line shapes obtained on a terbutylamine-borane complex (**3**, Scheme 1). Out of the investigated heteronuclear spin-pairs this actually showed the smallest residual dipolar coupling; such feature, however, is in excellent agreement with theoretical simulations based the quadrupole coupling constants observed for this complex at 77 K by pure nuclear quadrupole resonance (1.51 MHz and 1.57 MHz for the ^{11}B and ^{14}N, respectively),[38] in conjunction with the dipolar and J_{BN} couplings that were measured for the trimethylamine-borane complex.

C. Residual heteronuclear couplings in DAS and DOR NMR

Before concluding this discussion on the residual heteronuclear coupling effects that can be expected in the solid state NMR spectroscopy of quadrupoles, a brief reference is made to the results that will arise on using high resolution NMR techniques other than MQMAS. Particularly successful options toward achieving isotropic spectra from half-integer quadrupole nuclei have been DAS and DOR, techniques that focus solely on the central transition and which rely on either discreet or continuous changes of the sample spinning axis to remove the second-order quadrupole effects.[39] It is thus recalled that DAS achieves high resolution by correlating the S spin evolution at two consecutive spinning angles θ_S^1, θ_S^2 fulfilling

$$\frac{P_2(\cos\theta_S^2)}{P_2(\cos\theta_S^1)} = \frac{P_4(\cos\theta_S^2)}{P_4(\cos\theta_S^1)} = -\frac{t_1}{t_2} = -k, \tag{36}$$

and then subjecting the resulting data to a k-dependent shearing transformation [Fig. 1(B)]. DOR on the other hand rotates the sample simultaneously at the roots of both $P_2(\cos\theta)$ and $P_4(\cos\theta)$ such that

$$\langle P_2(\cos\theta)\rangle = \langle P_4(\cos\theta)\rangle = 0. \tag{37}$$

One-dimensional DOR acquisitions thus yield isotropic spectra simply by 1D Fourier transformation [Fig. 1(C)]. For the case of either technique the expressions that were derived earlier for the heteronuclear I-S coupling Hamiltonians and eigenvalues continue to be entirely valid; the only additional limitation that needs to be invoked is $m_S = \pm\frac{1}{2}$ due to central transition nature of these methods. Therefore, the isotropic multiplet positions that can be expected along the high resolution dimensions of these experiments will be given by

$$\nu(m_I) = \begin{cases} \frac{1}{2}\{\Delta[3m_I^2 - I(I+1)] + Jm_I\} & \text{for DOR} \\ \frac{1}{2}\left(\frac{1+k}{k}\right)\{\Delta[3m_I^2 - I(I+1)] + Jm_I\} & \text{for DAS} \end{cases} \qquad m_I = -I,\ldots,I \tag{38}$$

where Δ is as in Eq. (33) and the k-dependence in DAS arises from the shearing transformation that this technique involves. Such k values can range from 0.8 when $(\theta_S^1,\theta_S^2)=(39°,90°)$ to 5 for $(\theta_S^1,\theta_S^2)=(63°,0°)$; residual dipolar splittings can thus be expected to be smallest for the latter setting and largest for the former. Full numerical simulations of 2D DAS NMR experiments validate these predictions (Fig. 9); they also reveal a complex dependence of the anisotropic projection and of the overall 2D line shapes on the actual pair of complementary spinning angles that is chosen. This unusual behavior stems from the different weights with which the S-spin second-order quadrupolar and I-S first-order dipolar effects will appear along the two spectral dimensions depending on the spinning angles, and it apparently provides a sensitive insight on the relative orientation between dipolar and quadrupolar interactions. It is also worth remarking that the centers of mass of peaks along the isotropic projections of these numerical simulations differ by a less than half a Hz from the simple DAS predictions of Eq. (38). With regards to the DOR case, its extensive spatial averaging can be expected to remove—at least in the fast spinning regime—all the anisotropies involved in either the $H_D^{(1)}$ or $H_{Q,D}^{(2)}$ couplings; this would leave the isotropic residual given in the DOR version of Eq. (38) as the sole observable to be measured in these experiments.

V. RESIDUAL HOMONUCLEAR COUPLINGS IN MQMAS NMR

As mentioned, high resolution quadrupolar methods open up the possibility of detecting residual dipolar and J coupling effects also when identical nuclear species are involved. The theoretical treatment of these homonuclear cases, however, is substantially more involved than that of their heteronuclear counterparts due to the presence of extensive off-diagonal coupling terms stemming from secular flip-flop operators in the Hamiltonian. For instance for the simplest possible homonuclear situation amenable to experimental MQMAS NMR study, involving two identical spin-$\frac{3}{2}$ nuclei, the fast-spinning high-field coupling Hamiltonian will be given by

$$H_{IS}=J\bar{I}\cdot\bar{S}+H_{Q,D}^{(2)} \tag{39}$$

$$=\begin{pmatrix}
\frac{9}{2}\Delta_S+\frac{9}{2}\Delta_I+\frac{9}{4}J & 0 & 0 & 0 & 0 & 0 & 0 & 0 & 0 & 0 & 0 & 0 & 0 & 0 & 0 & 0 \\
0 & -\frac{9}{2}\Delta_S+\frac{3}{2}\Delta_I+\frac{3}{4}J & 0 & 0 & 6\Gamma_S^*+6\Gamma_I+\frac{3}{2}J & 0 & 0 & 0 & 0 & 0 & 0 & 0 & 0 & 0 & 0 & 0 \\
0 & 0 & -\frac{9}{2}\Delta_S-\frac{3}{2}\Delta_I-\frac{3}{4}J & 0 & 0 & 4\sqrt{3}\Gamma_I+\sqrt{3}J & 0 & 0 & 0 & 0 & 0 & 0 & 0 & 0 & 0 & 0 \\
0 & 0 & 0 & \frac{9}{2}\Delta_S-\frac{9}{2}\Delta_I-\frac{9}{4}J & 0 & 0 & -6\Gamma_S^*+6\Gamma_I+\frac{3}{2}J & 0 & 0 & 0 & 0 & 0 & 0 & 0 & 0 & 0 \\
0 & 6\Gamma_S+6\Gamma_I^*+\frac{3}{2}J & 0 & 0 & \frac{3}{2}\Delta_S-\frac{9}{2}\Delta_I+\frac{3}{4}J & 0 & 0 & 0 & 0 & 0 & 0 & 0 & 0 & 0 & 0 & 0 \\
0 & 0 & 4\sqrt{3}\Gamma_I^*+\sqrt{3}J & 0 & 0 & -\frac{3}{2}\Delta_S-\frac{3}{2}\Delta_I+\frac{1}{4}J & 0 & 0 & 4\sqrt{3}\Gamma_S^*+\sqrt{3}J & 0 & 0 & 0 & 0 & 0 & 0 & 0 \\
0 & 0 & 0 & -6\Gamma_S+6\Gamma_I^*+\frac{3}{2}J & 0 & 0 & -\frac{3}{2}\Delta_S+\frac{3}{2}\Delta_I-\frac{1}{4}J & 0 & 0 & 2J & 0 & 0 & 0 & 0 & 0 & 0 \\
0 & 0 & 0 & 0 & 0 & 0 & 0 & \frac{3}{2}\Delta_S+\frac{9}{2}\Delta_I-\frac{3}{4}J & 0 & 0 & -4\sqrt{3}\Gamma_S^*+\sqrt{3}J & 0 & 0 & 0 & 0 & 0 \\
0 & 0 & 0 & 0 & 0 & 4\sqrt{3}\Gamma_S+\sqrt{3}J & 0 & 0 & -\frac{3}{2}\Delta_S-\frac{9}{2}\Delta_I-\frac{3}{4}J & 0 & 0 & 0 & 0 & 0 & 0 & 0 \\
0 & 0 & 0 & 0 & 0 & 0 & 2J & 0 & 0 & \frac{3}{2}\Delta_S-\frac{3}{2}\Delta_I-\frac{1}{4}J & 0 & 0 & 6\Gamma_S^*-6\Gamma_I+\frac{3}{2}J & 0 & 0 & 0 \\
0 & 0 & 0 & 0 & 0 & 0 & 0 & -4\sqrt{3}\Gamma_S+\sqrt{3}J & 0 & 0 & \frac{3}{2}\Delta_S+\frac{3}{2}\Delta_I+\frac{1}{4}J & 0 & 0 & -4\sqrt{3}\Gamma_I+\sqrt{3}J & 0 & 0 \\
0 & 0 & 0 & 0 & 0 & 0 & 0 & 0 & 0 & 0 & -\frac{3}{2}\Delta_S+\frac{9}{2}\Delta_I+\frac{3}{4}J & 0 & 0 & -6\Gamma_S^*-6\Gamma_I+\frac{3}{2}J & 0 & 0 \\
0 & 0 & 0 & 0 & 0 & 0 & 0 & 0 & 0 & 6\Gamma_S-6\Gamma_I^*+\frac{3}{2}J & 0 & 0 & -\frac{9}{2}\Delta_S+\frac{9}{2}\Delta_I-\frac{9}{4}J & 0 & 0 & 0 \\
0 & 0 & 0 & 0 & 0 & 0 & 0 & 0 & 0 & 0 & -4\sqrt{3}\Gamma_I^*+\sqrt{3}J & 0 & 0 & \frac{9}{2}\Delta_S+\frac{3}{2}\Delta_I-\frac{3}{4}J & 0 & 0 \\
0 & 0 & 0 & 0 & 0 & 0 & 0 & 0 & 0 & 0 & 0 & -6\Gamma_S-6\Gamma_I^*+\frac{3}{2}J & 0 & 0 & \frac{9}{2}\Delta_S-\frac{3}{2}\Delta_I+\frac{3}{4}J & 0 \\
0 & 0 & 0 & 0 & 0 & 0 & 0 & 0 & 0 & 0 & 0 & 0 & 0 & 0 & 0 & -\frac{9}{2}\Delta_S-\frac{9}{2}\Delta_I+\frac{9}{4}J
\end{pmatrix}$$

where

$$\Delta_S=\sqrt{\frac{3}{2}}\frac{eQ_S}{2S(2S-1)h\omega_S^0}\langle R_{2,1}^{Q,S}R_{2,-1}^{D_{\rm eff}}+R_{2,-1}^{Q,S}R_{2,1}^{D_{\rm eff}}\rangle_{\rm MAS}, \tag{40a}$$

$$\Gamma_S=\frac{1}{2}\sqrt{\frac{3}{2}}\frac{eQ_S}{2S(2S-1)h\omega_S^0}\langle R_{2,-1}^{Q,S}R_{2,1}^{D_{\rm eff}}+R_{2,-2}^{Q,S}R_{2,2}^{D_{\rm eff}}\rangle_{\rm MAS}, \tag{40b}$$

$$\Gamma_S^*=\frac{1}{2}\sqrt{\frac{3}{2}}\frac{eQ_S}{2S(2S-1)h\omega_S^0}\langle R_{2,1}^{Q,S}R_{2,-1}^{D_{\rm eff}}+R_{2,2}^{Q,S}R_{2,-2}^{D_{\rm eff}}\rangle_{\rm MAS}, \tag{40c}$$

and analogous expressions hold for the definitions of Δ_I, Γ_I and Γ_I^*. This matrix stems from the explicit representation of Eqs. (17) and (19) in the coupled $\{|m_S,m_I\rangle\}$ Zeeman product basis set and is expected to grow as $[(2S+1)(2I+1)]^2$ depending on the spin numbers involved: 16×16 for

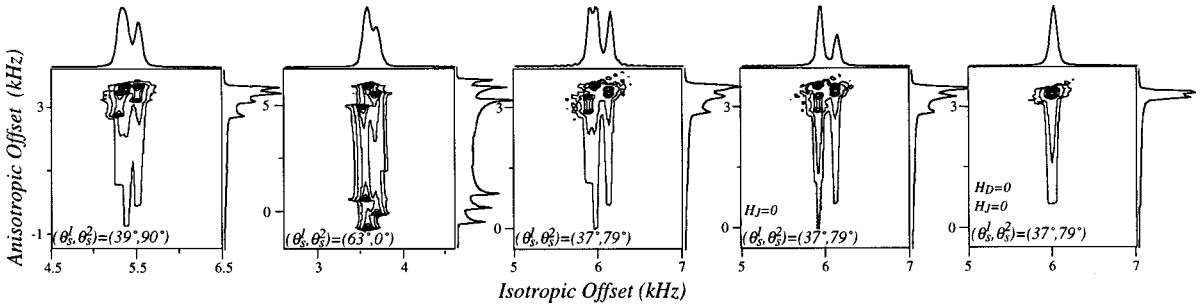

FIG. 9. 2D DAS line shapes expected from isolated $S=\frac{3}{2}$, $I=1$ spin pairs as a function of different complementary (θ_S^1,θ_S^2) spinning angles. Shown on the vertical and horizontal axes are the isotropic and anisotropic projections arising from these suitably sheared data. Also illustrated for the (37°, 79°) DAS case are the effects of sequentially removing the dipolar- and *J*-coupling effects, leading to a purely quadrupolar *S* spectrum. All spectra were calculated on the basis of a ^{11}B–^{14}N spin pair at 4.7 T possessing all parameters as measured on the trimethylamine-borane complex, as well as isotropic and anisotropic ^{11}B shifts of -30 and 0 ppm, respectively.

$I=S=\frac{3}{2}$, 36×36 for $I=S=\frac{5}{2}$, etc. Furthermore, its effects on the final spectra can only be properly described when considered in unison with the potentially more important shielding and quadrupolar effects that may dominate the diagonal in this sort of representation.

To circumscribe somewhat the very wide diversity of scenarios that are then open to analysis in these homonuclear coupling situations, we assume for this discussion that the two coupled sites of interest are chemically equivalent. This establishes a common relation between the sets of Euler angles $(\alpha,\beta,\gamma),(a,b,c)$ orienting the two quadrupole tensors with respect to the internuclear dipolar vector, while allowing us to disregard—at least in the fast spinning regime—the effects of chemical shifts on the spectral line shapes. For the actual forms of the various spatial spherical tensor components in the Hamiltonians the angular definitions given in Eq. (24) were still employed, leading to the relations given in Eqs. (25)–(27) and (A1)–(A10). With the aid of these conventions a ''brute-force'' numerical calculation on the influence of these coupling effects on MQMAS NMR line shapes was undertaken. These spectra were obtained by Fourier processing the weighted powder average arising from the calculated bidimensional time-domain signals

$$S(t_1,t_2)=\sum_{A=I,S}\sum_{m_B=m_S,m_I}|\langle m,m_B|A_+^{2m}|-m,m_B\rangle|^2|\langle\tfrac{1}{2},m_B|A_+|-\tfrac{1}{2},m_B\rangle|^2\times e^{i\{[E(m,m_B)-E(-m,m_B)]t_1+[E(\frac{1}{2},m_B)-E(-\frac{1}{2},m_B)]t_2\}}. \tag{41}$$

This expression is the homonuclear analog of Eq. (22); in it the indices A and B refer to the two different spins, A_+^{2m} denotes the $-m_A\leftrightarrow+m_A$ multiquantum ladder operator, and both eigenstates and eigenvalues refer to the diagonalization of the total Hamiltonian

$$(H_{Q,I}^{(1)}+H_{Q,S}^{(1)}+H_{Q,I}^{(2)}+H_{Q,S}^{(2)}+H_{Q,D}^{(2)}+H_J)|m_A,m_B\rangle=E(m_A,m_B)|m_A,m_B\rangle. \tag{42}$$

Figure 10 illustrates some of the effects that on the basis of this model can be expected to arise in the MQMAS line shapes of spin-$\frac{3}{2}$ pairs as a result of introducing the homonuclear dipolar and *J* couplings. When viewed in terms of the quadrupolar/Zeeman ratio $eQ_S/[2S(2S-1)\hbar\omega_S^0]$, these homonuclear coupling effects are comparable to their heteronuclear counterparts. Even more noticeable effects can be

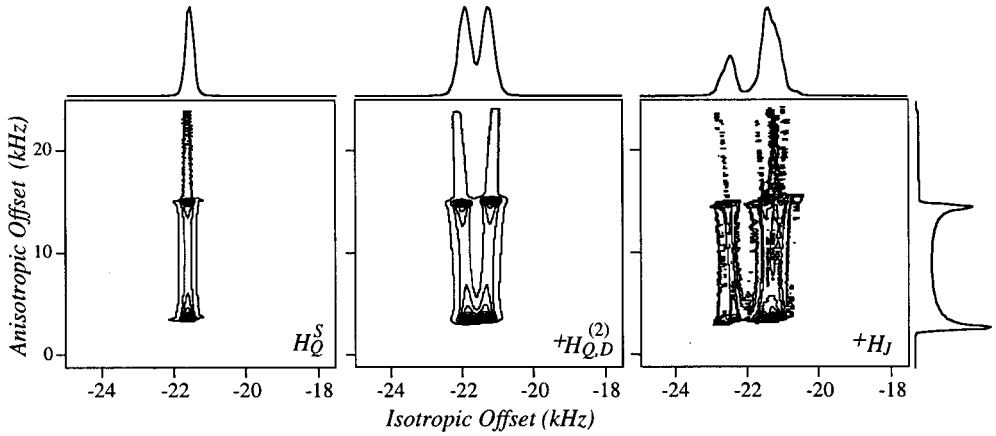

FIG. 10. Effects expected from the introduction of residual dipolar and of additional *J* couplings on the 2D MQMAS NMR line shapes arising from a homonuclear $S=I=\frac{3}{2}$ spin pair. Spectra were calculated for the case of axially symmetric and equivalent ^{11}B spins that are 1.5 Å apart in a B_0 field of 4.7 T, with an e^2qQ/h of 5 MHz, a *J* coupling of 100 Hz and a natural line width of 20 Hz. 1D traces correspond to projections along the isotropic and anisotropic axes.

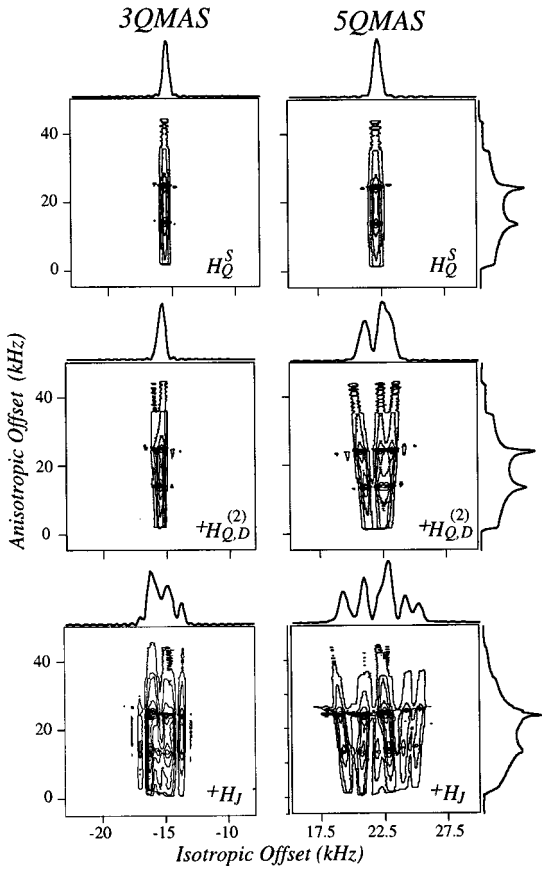

FIG. 11. Idem as in Fig. 10 but for the 3QMAS and 5QMAS NMR spectra of two coupled spin-$\frac{5}{2}$ (^{55}Mn–^{55}Mn at 4.7 T, 1.5 Å apart, $e^2qQ/h = 12$ MHz, $\eta_Q = 0.5$, $J = 100$ Hz).

expected when exploring higher-order MQ transitions, as illustrated in Fig. 11 for the case of a spin-$\frac{5}{2}$. Unfortunately, under the relatively strong quadrupole coupling conditions needed for a clear observation of these effects the signal-to-noise ratio of MQMAS experiments may also be expected to be relatively poor. In spite of this consideration, the effects of these homonuclear couplings can be observed even at moderate magnetic fields. Figure 12 for instance illustrates the experimental 2D ^{11}B MQMAS NMR results obtained on investigating a bispinacolato diborane complex (**4**, Scheme 1). The x-ray diffraction analysis of this compound shows the two directly bonded boron sites related by symmetry and at a 1.71 Å distance;[40] given the ^{11}B quadrupolar coupling parameters $e^2qQ/h = (2.5 \pm 0.1)$ MHz and $\eta_Q = (0.9 \pm 0.1)$ that become available from fitting the MQMAS data, a broadening that is evident on projecting the experimental data into the isotropic domain of the sheared 2D MQMAS spectrum results. A complete fitting of the data also leads to relative tensor orientations $(\alpha,\beta) = (a,b) = (0°,0°)$—in accordance with the sites' symmetry about the B–B axis—to a large but not unusual $J = (85 \pm 20)$ Hz indirect coupling,[41] and to a relatively small natural linewidth contribution. Agreement between the theoretical expectations and experimental line shapes also improves slightly on considering that one in every five ^{11}B is actually heteronuclearly coupled to a ^{10}B ($I = 3$), for which Zeeman quadrupole and coupling effects are fixed by the relative ratio between the nuclear quadrupole and magnetic dipole moments of ^{11}B and ^{10}B. The results of all these considerations are summarized by the simulations shown on the bottom row of Fig. 12. As in the simpler heteronuclear cases, agreement between these theoretical predictions and the experimental observations is quite satisfactory.

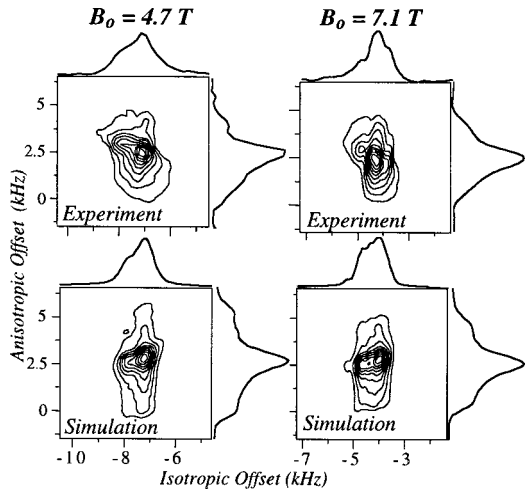

FIG. 12. Comparisons between the experimental MQMAS NMR line shapes observed for the bispinacolato diborane complex at different magnetic fields, and corresponding best fit simulations calculated for an $I = S = \frac{3}{2}$ pair as described in the text.

Finally, Fig. 13 illustrates a similar comparison for the case of two mutually coupled spin-$\frac{5}{2}$ nuclei: the ^{55}Mn sites in dimanganese decacarbonyl (**5**, Scheme 1). The 3.05 MHz quadrupole coupling constant reported in the literature for the two ^{55}Mn sites in this complex[42] is in very good agreement with the value extracted from the 2D MQMAS spectra (3.01 ± 0.05 MHz), which also reveals an $\eta_Q = 0.5 \pm 0.1$ asymmetry parameter. Mn–Mn coupling effects are clearly evident on inspecting the line shape resulting along the

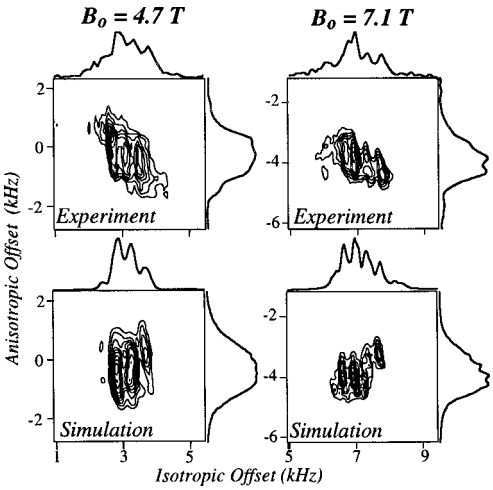

FIG. 13. Idem as in Fig. 12 but for the dimanganese decacarbonyl complex ($I = S = \frac{5}{2}$, 3Q MAS NMR). The minor differences between the relative intensities displayed by the simulated and experimental 2D line shapes are ascribed to inhomogeneities in the excitation of the powder crystallites (unaccounted for in the simulations, see text).

MQMAS isotropic dimension; in fact some of these are even discernible on the regular 1D MAS second-order powder pattern. According to the 2.895 Å intermetal distance reported in the x-ray diffraction analysis of this compound, however,[43] homonuclear dipolar coupling effects will actually be relatively minor under the employed experimental conditions; this in turn explains the weak field dependence displayed by the ^{55}Mn MQMAS NMR spectra. That the source of these splittings is mainly indirect in nature is validated by numerical fits of the spectra, which match experiments fairly well with $J=(65\pm5)$ Hz, $\Delta J\approx 0$. Still, calculations indicate that a consequence of the nonsecular dipolar couplings at the explored magnetic field strengths is to alter the relative widths (and thus the heights) of the various components in the 2D multiplet.

VI. CONCLUSIONS

The main goal of the present study was to discuss the basic theory underlying the occurrence of nonsecular dipolar couplings between quadrupolar nuclei, and to demonstrate the feasibility of experimentally observing and characterizing these effects in isolated spin-pairs with the aid of recently developed high resolution NMR techniques. For deriving such theories we relied on the considerable body of work that has been developed for understanding similar effects in the case of quadrupolar/spin-$\frac{1}{2}$ heteronuclear pairs, particularly when these can be treated under the high B_0 field approximation. For the case of coupling between quadrupoles a considerably wider variety of research avenues opens up for exploration, as a result of the many different 1D and 2D NMR experiments capable of affording high resolution spectra and of the possibility of dealing with either hetero- or homonuclear spin systems. Some of these research avenues were explored in this study, even if for the sake of clarity most of the discussion focused on the MQMAS NMR line shapes that can be expected on analyzing isolated spin-pairs. The presented data show that analyses of this kind can indeed yield novel spectral line shapes, and carry a structural and coupling information that may hitherto have been difficult to characterize from powders by other means. It is also worth remarking that even with the constraints laid out during the course of this study, many of the Hamiltonians that were derived in it can be exploited for evaluating the results that will be afforded by non-MQMAS experiments or the line shapes that will arise from multinuclear ensembles of coupled spins. In fact the high-field formalism developed in this paper can be extended in a relatively straightforward manner to enable the numerical evaluation of these effects for arbitrary quadrupole/Zeeman ratios, and for samples subjected to a variety of spinning angles or speeds. Some of the predictions stemming from these additional investigations are currently being explored.

ACKNOWLEDGMENTS

We are grateful to Dr. Veronica Frydman (UIC) for the purification and characterization of all compounds used in this work, and to Dr. S. Wimperis (University of Oxford) for making us aware of his results in this area. This work was supported by the National Science Foundation through Grants Nos. DMR-9806810 and CHE-9841790 (Creativity Extension Award). This work was presented in part at the 41st Rocky Mountains NMR Conference (Denver, CO, July 1999); poster #320. L.F. is a Camille Dreyfus Teacher-Scholar (1996–2001), University of Illinois Junior Scholar (1997–2000), Alfred P. Sloan Fellow (1997–2000).

APPENDIX

The spatial anisotropies of all terms in the second-order interaction Hamiltonians given in Eqs. (18) and (19) are a function of the spherical tensor components $\{R^{\lambda}_{2,m}\}_{m=\pm1,\pm2,}$ with λ representing the *S* quadrupolar, *I* quadrupolar or *I-S* dipolar interactions. The angular relations between the PAS's of these various spin couplings are laid out in Eq. (24). The purpose of this Appendix is to summarize the actural expressions of the $\{R^{\lambda}_{2,m}\}$ for the various λ-interactions as well as their average values in the fast spinning regime; these expressions may be retrieved electronically from AIP's EPAPS homepage (see Ref. 44).

[1] J. Schaefer and E. O. Stejskal, J. Am. Chem. Soc. **98**, 1031 (1976).
[2] E. R. Andrew, A. Bradbury, and R. G. Eades, Nature (London) **182**, 1659 (1958).
[3] I. J. Lowe, Phys. Rev. Lett. **2**, 285 (1959).
[4] R. K. Harris and A. C. Olivieri, Prog. Nucl. Magn. Reson. Spectrosc. **24**, 435 (1992).
[5] R. K. Harris, in *Encyclopedia of NMR*, edited by D. M. Grant and R. K. Harris (Wiley, New York, 1995), p. 2909.
[6] D. L. V. d. Hart, H. S. Gutowsky, and T. C. Farrar, J. Am. Chem. Soc. **89**, 5056 (1967).
[7] S. J. Opella, H. M. Frey, and T. A. Cross, J. Am. Chem. Soc. **101**, 5856 (1979).
[8] C. J. Groombridge, R. K. Harris, K. J. Packer, B. J. Say, and S. F. Tanner, J. Chem. Soc. Chem. Commun. **1980**, 174.
[9] A. Naito, S. Ganapathy, and C. A. McDowell, J. Chem. Phys. **74**, 5393 (1981).
[10] J. G. Hexem, M. H. Frey, and S. J. Opella, J. Chem. Phys. **77**, 3847 (1982).
[11] A. C. Olivieri, L. Frydman, and L. E. Diaz, J. Magn. Reson. **75**, 50 (1987).
[12] A. C. Olivieri, L. Frydman, M. Grasselli, and L. E. Diaz, Magn. Reson. Chem. **26**, 615 (1988).
[13] A. C. Olivieri, J. Magn. Reson. **81**, 201 (1989).
[14] G. Wu and R. E. Wasylishen, Mol. Phys. **95**, 1177 (1998).
[15] A. Samoson, E. Lippmaa, and A. Pines, Mol. Phys. **65**, 1013 (1988).
[16] K. T. Mueller, B. Q. Sun, G. C. Chingas, J. W. Zwanziger, T. Terao, and A. Pines, J. Magn. Reson. **86**, 470 (1990).
[17] L. Frydman and J. S. Harwood, J. Am. Chem. Soc. **117**, 5367 (1995).
[18] J. McManus, R. Kemp-Harper, and S. Wimperis, Chem. Phys. Lett. (in press).
[19] A. Medek, J. S. Harwood, and L. Frydman, J. Am. Chem. Soc. **117**, 12779 (1995).
[20] P. K. Madhu, A. Goldbourt, L. Frydman, and S. Vega, Chem. Phys. Lett. **307**, 41 (1999).
[21] D. Massiot, B. Touzo, D. Trumeau, J. P. Coutures, J. Virlet, P. Florian, and P. J. Grandinetti, Solid State Nucl. Magn. Reson. **6**, 73 (1996).
[22] A. Abragam, *Principles of Nuclear Magnetism* (Oxford University Press, Oxford, 1961).
[23] R. E. Wasylishen, in *Encyclopedia of Nuclear Magnetic Resonance*, edited by D. M. Grant and R. K. Harris (Wiley, New York, 1995), p. 1685.
[24] U. Haeberlen, in *Advances in Mangetic Resonance*, edited by J. S. Waugh (Academic, New York, 1976), Supplement 1.
[25] C. P. Slichter, *Principles of Nuclear Magnetic Resonance* (Springer-Verlag, New York, 1990).
[26] L. D. Landau, *Quantum Mechanics* (Pergamon, Oxford, 1991).
[27] S. Ding and C. A. McDowell, J. Chem. Phys. **107**, 7762 (1997).
[28] G. Wu, S. Kroeker, R. E. Wasylishen, and R. G. Griffin, J. Magn. Reson. **124**, 237 (1997).

[29] A. Medek, L. Marinelli, and L. Frydman, in *Solid State NMR of Inorganic Materials*, edited by J. J. Fitzgerald, ACS Symp. Series (Washington, DC; 1999), Vol. 717, p. 136.
[30] S. P. Brown and S. Wimperis, J. Magn. Reson. **128**, 42 (1997).
[31] S. Ganapathy, S. Schramm, and E. Oldfield, J. Chem. Phys. **77**, 4360 (1982).
[32] D. Freude and J. Haase, *NMR Basic Principles and Progress* (Springer, Heidelberg, 1993), Vol. 29.
[33] Z. Gan and D. M. Grant, J. Magn. Reson. **90**, 522 (1990).
[34] E. C. Reynhardt, J. Phys. C **19**, 1823 (1986).
[35] M. Kameda and G. Kodama, Inorg. Chem. **23**, 3710 (1984).
[36] W. Kasten, H. Dreizler, and R. L. Kuczkowski, Z. Naturforsch. A **40**, 1262 (1985).
[37] T. Schaefer, R. Sebastian, and S. R. Salma, Can. J. Chem. **59**, 3026 (1981).
[38] A. Lötz, E. Palange, and J. Vöitlander, J. Magn. Reson. **50**, 417 (1982).
[39] E. W. Wooten, K. T. Muller, and A. Pines, Acc. Chem. Res. **25**, 209 (1992).
[40] H. Nöth, Z. Naturforsch. B **39**, 1463 (1984).
[41] J. D. Kennedy, in *Multinuclear NMR*, edited by J. Mason (Plenum, New York, 1987), p. 221.
[42] E. A. C. Lucken and D. F. Williams, Proc. Colloq. Amp. **14**, 1121 (1966).
[43] M. Martin, B. Rees, and A. Mitschler, Acta Crystallogr., Sect. B: Struct. Crystallogr. Cryst. Chem. **38**, 6 (1982).
[44] See EPAPS Document No. E-JCPSA6-112-025003 for a description of the spatial components for the various interactions. This document may be retrieved via the EPAPS homepage (http://www.aip.org/pubservs/epaps.html) or from ftp.aip.org in the directory /epaps/. See the EPAPS homepage for more information.